Fermilab FERMILAB-FN-734 April 2003

Beam Loss and Backgrounds in the CDF and DØ Detectors due to Nuclear Elastic Beam-Gas Scattering*

A.I. Drozhdin, V.A. Lebedev, N.V. Mokhov, L.Y. Nicolas†,
D.V. Sidorov‡, S.I. Striganov, A.V. Tollestrup
Fermi National Accelerator Laboratory
P.O. Box 500, Batavia, Illinois 60510
† *Also University of Glasgow, UK*
‡ *Moscow State University, Moscow, Russia*

April 10, 2003

Abstract

Detailed simulations were performed on beam loss rates in the vicinity of the Tevatron Collider detectors due to beam-gas nuclear elastic interactions. It turns out that this component, not intercepted by the Tevatron collimation system, can drive the accelerator-related background rates in the CDF and DØ detectors, exceeding those due to outscattering from collimator jaws, inelastic beam-gas interactions and other processes. Results of realistic simulations with the STRUCT and MARS codes are presented for the interaction region components, forward proton detectors and the CDF and DØ subdetectors. Beam loss induced background rates calculated in the CDF West beam halo monitors are in a good agreement with recent measurements. It is shown that a steel mask in the Roman Pot station region can reduce the background rates at the collider detectors by almost an order of magnitude.

*Work supported by the Universities Research Association, Inc., under contract DE-AC02-76CH00300 with the U. S. Department of Energy.

1 Introduction

Even in good operational conditions in an accelerator, some particles leave the beam core producing a beam halo. This happens because of beam-gas interactions, intra-beam scattering, proton-antiproton collisions in the interaction regions (IP), and particle diffusion due to RF noise, ground motion and resonances excited by the accelerator magnet nonlinearities and power supplies ripple. As a result of halo interactions with limiting apertures, hadronic and electromagnetic showers are induced in accelerator and detector components causing excessive backgrounds in the detectors. Only with a very efficient beam collimation system can one reduce uncontrolled beam losses in the machine to an allowable level [1, 2, 3]. A new two-stage collimation system has been developed for the Tevatron Run II [4] for beam cleaning of slowly growing transverse and longitudinal halo.

About 0.1% of protons and antiprotons hitting the collimators are scattered back into the beam pipe and later lost on limiting apertures, in most cases upstream of the CDF and DØcollider detectors. Products of beam-gas interactions not intercepted by the collimation system have also a good chance to be lost at the same locations in front of the IPs. The main process of beam-gas interaction, a multiple Coulomb scattering, results in slow diffusion of protons (antiprotons) from the beam core causing emittance growth. These particles increase their betatron amplitudes gradually during many turns and are intercepted by collimators before they reach other limiting apertures. In inelastic nuclear interactions of a beam with residual gas, leading nucleons are generated at angles large enough for them – along with other secondaries – to be lost within tens of meters after such interactions. Nuclear elastic beam-gas scattering can result in a substantial increase of the betatron amplitude. It turns out that in the Tevatron many of these particles are not intercepted by the main collimators, and about 25% of them are lost in the vicinity of the IPs adding to the detector background.

A multi-turn particle tracking through the accelerator with halo interactions with the collimators and elastic beam scattering on the residual gas is conducted with the STRUCT code [5]. All the lattice components with their real strengths and aperture restrictions are taken into account. Using the beam loss distributions calculated this way in the vicinity of the Tevatron's IPs, detailed hadronic and electromagnetic shower simulations with the MARS14 code [6] are performed in the machine, detector and tunnel components as well as in surrounding dirt, experimental halls and their shielding. It is found that short steel collimators/masks in the IPs would substantially reduce detector backgrounds induced by nuclear elastic beam-gas scattering.

2 Scraping Rate

The ultimate Tevatron Run II parameters relevant to this consideration include 36 bunches of 2.7×10^{11} protons and 1.35×10^{11} antiprotons each, with normalized horizontal emittances of 20 mm-mrad and 15 mm-mrad, respectively. The total beam intensities at the beginning of the store are $N_p = 9.72\times10^{12}$ and $N_{\overline{p}} = 4.86\times10^{12}$. The ultimate luminosity at the beginning of the store would be 3.31×10^{32} cm^{-2}s^{-1} averaging to 1.43×10^{32} cm^{-2}s^{-1} over a 13.5-hour store. Fig. 1 shows numerically estimated evolution of beam loss over such a store for three major components:

1. $\overline{p}p$ collisions at two IPs (*collision loss*), $\Delta I = 2.2\times10^7$ p/s or $\overline{p}$/s.
2. Particle loss from the RF bucket due to heating of a longitudinal degree of freedom (*longitudinal loss*), $\Delta I = 2\times10^7$ p/s and 6.1×10^6 $\overline{p}$/s.
3. *Beam-gas scattering*, $\Delta I = 6.5\times10^6$ p/s and 2.9×10^6 $\overline{p}$/s, calculated at a nitrogen equivalent pressure of 10^{-9} torr with the following gas content (in nanotorr): H_2 (5.7), CO (0.14), N_2 (0.07), C_2H_2 (0.06), CH_4 (0.11), CO_2(0.07), Ar (0.09).

The beam loss rates ΔI given above are those for 36 bunches averaged over a 13.5-hour store. Taken in these calculations inelastic $\overline{p}p$ cross section is σ_{in} = 60 mb at $\sqrt{s}$=2 TeV, while σ_{el} = 15 mb. As shown in Ref. [7], about 40% of protons (antiprotons) elastically scattered at the Tevatron IPs remain in the 3σ core after a bunch-bunch collision. Therefore, the inelastic and 60% of elastic events contribute to *collision loss*. Fig. 1 shows also the evolution of proton and antiproton bunch intensities, and Fig. 2 gives resulting beam intensity behavior. Corresponding intensity drops over a 13.5-hour store are 26% and 34% for proton and antiproton beams, respectively. Longitudinal beam loss, beam gas-scattering and elastic part of collision loss are the main mechanisms of the slow beam halo growth. The main collimation system (see [4] and next section) is designed to intercept about 99.9% of this halo. The above calculations give one N_{sp} = 2.93×10^7 p/s and $N_{s\overline{p}}$ = 1.15×10^7 $\overline{p}$/s as the scraping rates for proton and antiproton beams, correspondingly. Note, that N_{sp} is very close to 3×10^7 p/s derived in Ref. [4], while $N_{s\overline{p}}$ is about a factor of two higher because of a higher antiproton beam intensity used in the current analysis. It is assumed in this study that N_{sp} = 3×10^7 protons per second interact with the primary collimators, equally splitted between horizontal, vertical and off-momentum ones.

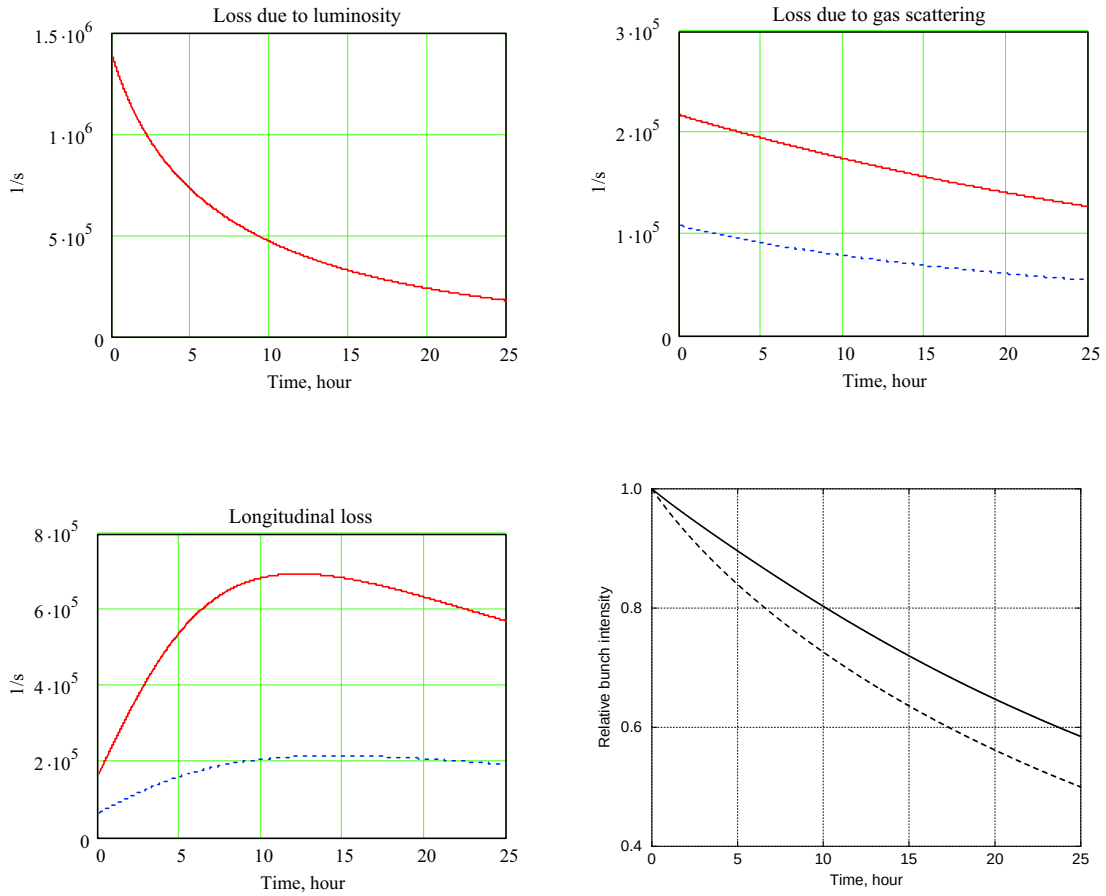

Figure 1: Evolution of proton (solid curves) and antiproton (dashed curves) bunch loss rates – collision (left top), longitudinal (left bottom) and beam-gas (right top) – and relative bunch intensity as evolved in a store (right bottom).

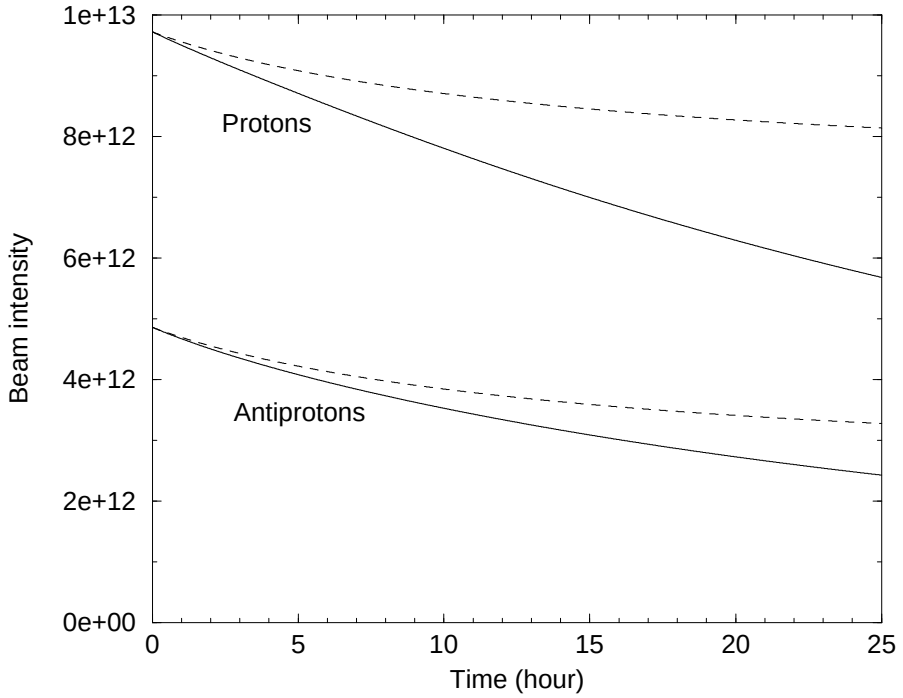

Figure 2: Proton and antiproton beam intensity evolution over a store. Dashed curves show intensity behavior with collision loss only.

3 Run II Collimation System

The Run II collimation system is described in detail in Ref. [4]. It is based on a two-stage collimation approach [1, 2, 8] to localize most of losses in the straight sections D49, EØand F17. For each beam, the system consists of a thin primary collimator (scatterer) and two secondary collimators placed with optimal phase advances. As a result of a kick generated in primary collimators, the halo particle impact parameter on secondary collimators is so large that only a tiny fraction of them outscatters back to the aperture, resulting in a very high scraping efficiency. This also decreases secondary collimator jaw overheating and mitigates alignment requirements. The β-functions, dispersions and phase advances for the collimator locations are presented in Table 1. Collimator positions in the Tevatron ring are shown in Fig. 3. Parameters of the scatterers and secondary collimators have been carefully optimized for the Tevatron beams [3, 4, 9]. The 5-mm thick tungsten primary collimators for proton and antiptoton beams are positioned at 5σ from the beam axis both in vertical and horizontal planes. The 1.5-m long stainless steel secondary collimators consist of L-shape jaws positioned at 6σ from the beam axis in both planes. The proton and antiproton spatial distributions at the primary and secondary collimators are shown in Fig. 4. Numerical simulations are done for the Tevatron lattice [10] in the presence of the proton and antiproton orbit separation designed for Run II [11].

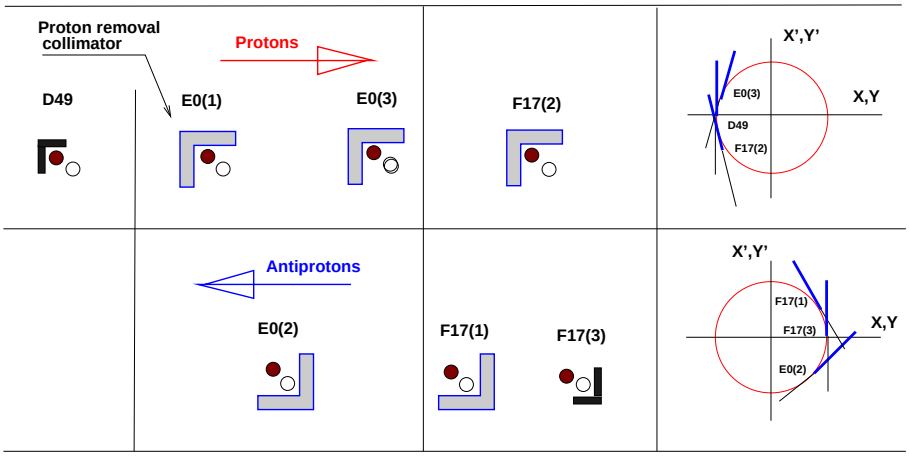

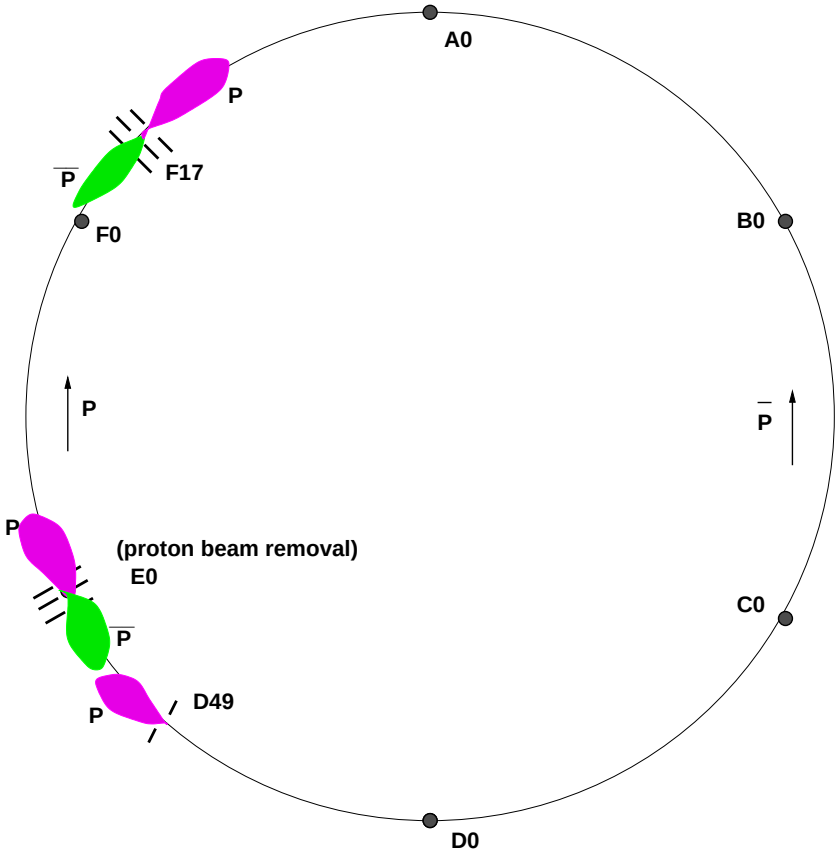

Figure 3: Tevatron Run-II beam collimation system.

Table 1: β-functions, dispersions and phase advances between primary and secondary collimators.

Collimator	β-function (m)		Dispersion (m)	Phase advance between primary and secondary collimators (deg)	
	horizontal	vertical		horizontal	vertical
D49 primary (p)	84.8	74.1	1.8	0	0
E03 secondary (p)	96.3	58.6	2.4	45	41
F172 secondary (p)	88.0	36.8	5.6	340	344
F173 primary ($\overline{p}$)	61.5	50.0	4.9	0	0
F171 secondary ($\overline{p}$)	94.8	34.1	5.8	7	12
E02 secondary ($\overline{p}$)	93.3	59.0	2.3	300	313

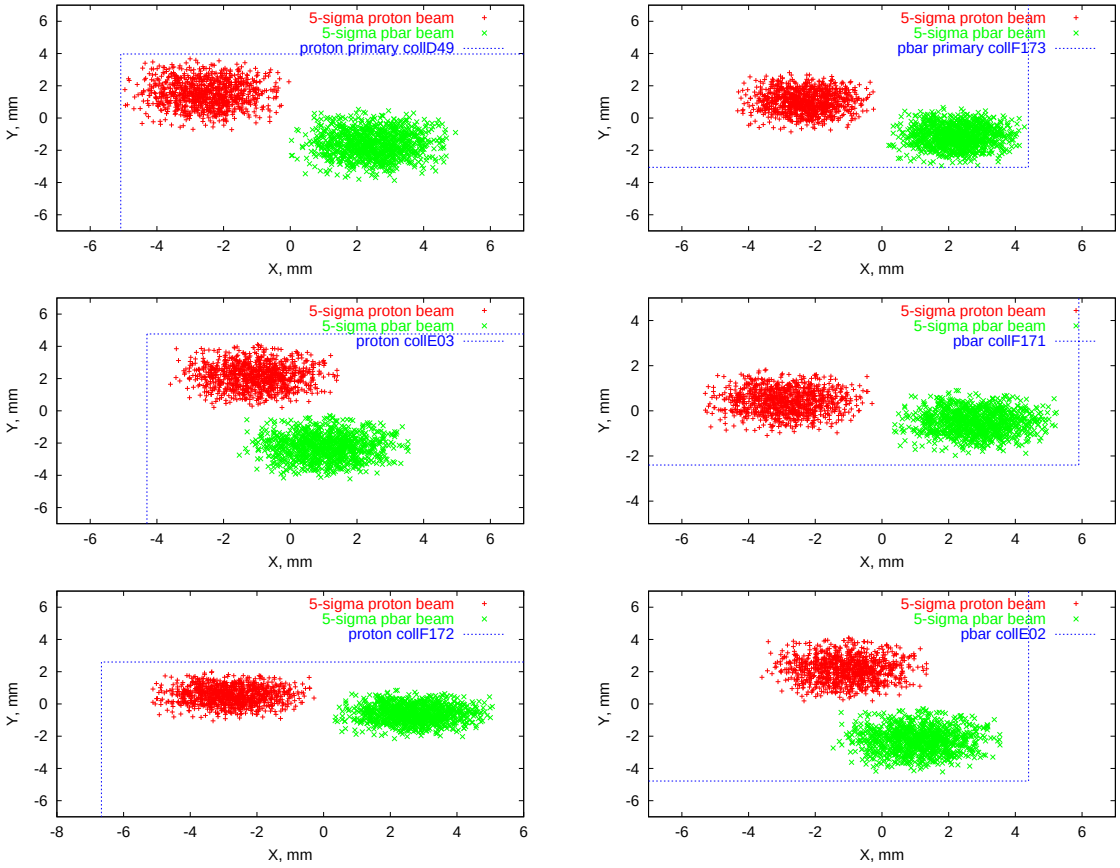

Figure 4: The 5-σ proton (red (black)) and antiproton (green (grey)) spatial distributions. *Left:* at proton primary collimator D49 (top) and secondary collimators E03 (middle) and F172 (bottom). *Right:* at antiproton primary collimator F173 (top) and secondary collimators F171 (middle) and E02 (bottom).

4 Beam Loss due to Slow Halo Growth

The transverse emittance growth measured in Tevatron [12] is approximately 0.25 πmm-mrad/hr. A transverse diffusion coefficient is about 2×10^{-6} mm^2/s. The corresponding transverse diffusion velocity of protons (antiprotons) from the beam core is about 1.5 μm/s. Based on [12, 13, 14] we assume that at slow increase of halo particle betatron amplitude or slow change in $\Delta p/p$, halo would interact with a primary collimator with a small impact parameter of 0.1-0.5 μm. As a result of multiple Coulomb scattering in this process, the impact parameter of this particle at a secondary collimator increases to about 0.1-0.3 mm. Horizontal and vertical phase space at the proton primary and secondary collimators are presented in Fig. 5. Large amplitude protons are intercepted by the secondary collimators during the first turn after interaction with the primary collimator. Protons (antiprotons) with amplitudes smaller than 6σ survive during several tens of turns until they increase amplitude in next interactions with primary collimators. These particles produce a secondary halo and occupy the 6σ envelope. In Tevatron, beam halo particles interact with primary collimators 2.2 times on average.

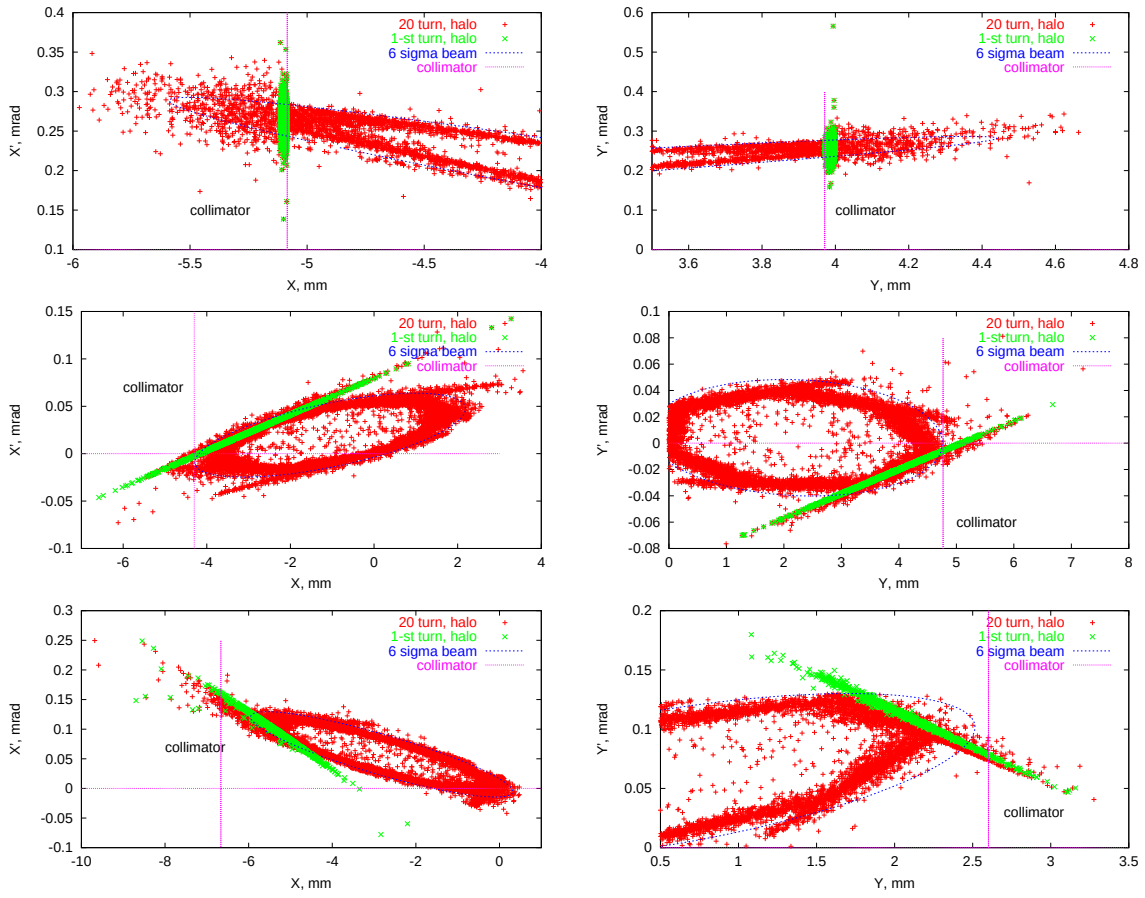

Figure 5: Horizontal (left) and vertical (right) phase space at primary proton collimator D49 (top), and secondary collimators E03 (middle) and F172 (bottom). Green (grey) – halo particles at the first turn after interaction with the primary collimator, red (black) – secondary halo, blue (black line) – 6σ envelope.

Next to the collimators limiting apertures in the Tevatron are Roman Pots (RP) of the DØand CDF forward detectors [3] sitting at 8-10$\sigma_{x,y}$ and 15σ_x, respectively. Corresponding direct proton halo hit rates are about (1-3)$\times 10^5$ p/s in the DØRPs and approximately a factor of ten lower in the CDF RPs. Halo interactions with RPs can contribute to undesirable backgrounds in the main detectors. Calculated beam loss distributions with collimators and RPs in their working positions are shown in Fig. 6. About 0.08% of the scraping rate N_{sp} is lost in 60-m regions upstream of the DØand CDF detectors: 3.5×10^{-4} p/s or 0.0056 W in BØand 2.4×10^{-4} p/s or 0.0038 W in DØ. These protons are lost predominantly in the separators and three dipoles adjacent to the low-β quadrupoles.

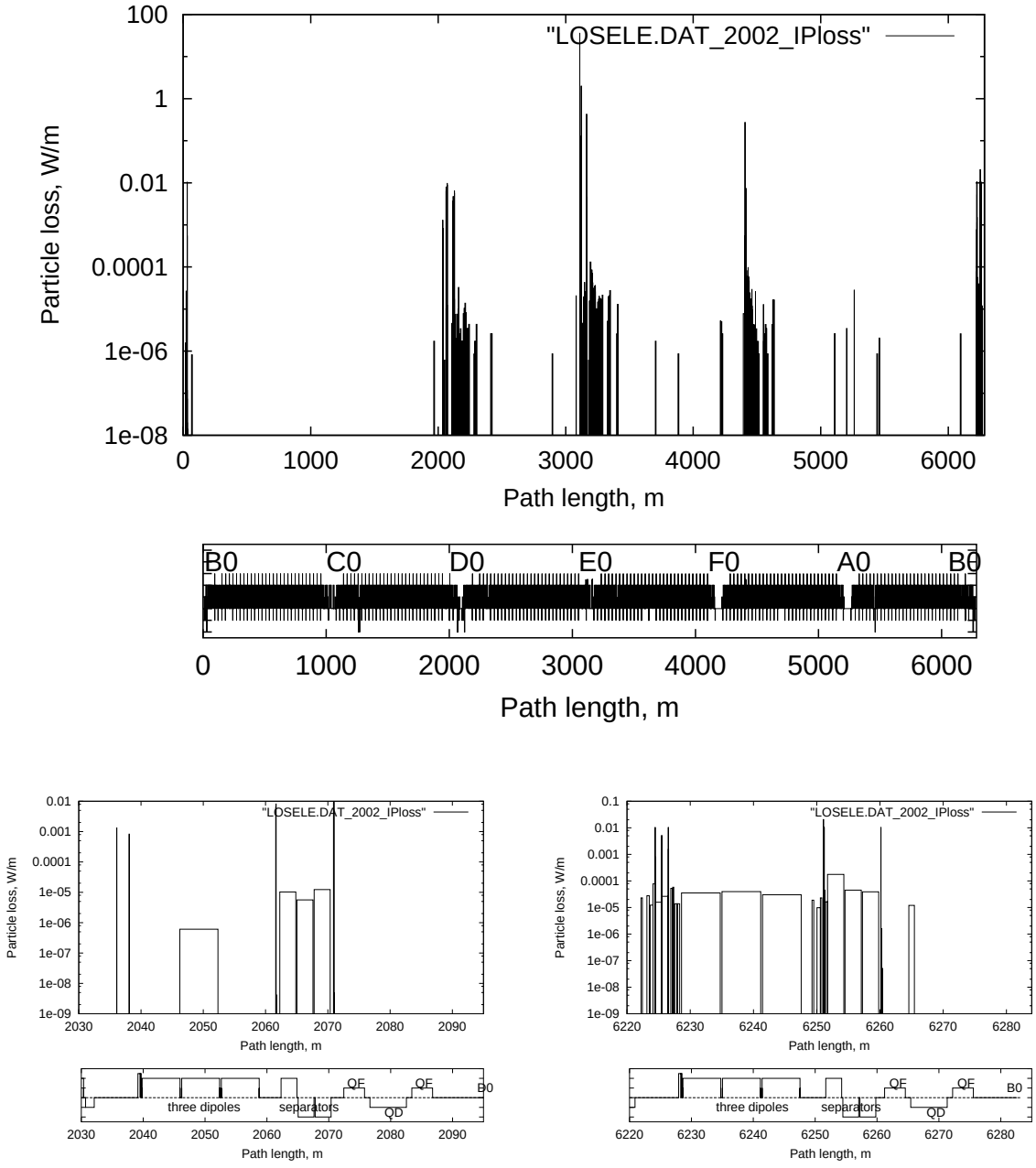

Figure 6: Beam loss distribution in the entire ring (top) and in the DØand BØregions (bottom).

5 Proton-Nucleus Elastic Scattering

As mentioned above, products of inelastic interactions of the beam with residual gas nuclei are lost within tens of meters after such interactions (see also Ref. [7]). At the same time, scattering angles in nuclear elastic beam-gas interactions are small enough for protons to travel much larger distances in the lattice and – if not intercepted by collimators – resulting in their loss on limiting apertures. A differential cross section of proton-nucleus (pA) elastic scattering can be parameterized as

$$d\sigma/dq^2 = \sigma_{el} B_{el} exp(-B_{el} q^2) + \sigma_{qel} B_{qel} exp(-B_{qel} q^2), \quad (1)$$

where $q = p\theta$, p is a proton momentum, θ is a scattering angle, σ_{el} and B_{el} are a total cross section and slope of the coherent pA elastic scattering from the nucleus as a whole, σ_{qel} and B_{qel} are a total cross section and slope of the incoherent pA elastic scattering (scattering which excites or breaks up the nucleus). Total cross sections of these processes are calculated using the Glauber model with inelastic corrections. For a 1-TeV proton on nitrogen, σ_{el} = 115 mb and σ_{qel} = 25 mb. The slope of the coherent scattering is almost independent of energy and can be taken from [15] as $B_{el} = 12.85 * A^{2/3}$ GeV^{-2}. The slope of the incoherent scattering is the same as in the pp elastic scattering: $B_{qel} = 11.04$ GeV^{-2} at 1 TeV. Differential cross section of proton-nitrogen elastic scattering at 1 TeV is shown in Fig. 7 (left) along with a Coulomb scattering contribution calculated from the Rutherford cross section with a Gaussian nuclear form-factor. Note that a total macroscopic cross section of the later process is 8478 cm^2/g, i.e. about 100 times larger than the corresponding elastic cross section. The quality of this formalism is demonstrated in Fig. 7 (right) where one can see a good agreement with data [15]. Using the above formulae, one can calculate a probability for proton to scatter elastically on nitrogen to an angle larger than θ_{min} due to strong interactions

$$W(\theta \geq \theta_{min}) = 1.08 \cdot 10^{-3} (exp(-11.04 \cdot q^2_{min}) + 4.6 \cdot exp(-74.46 \cdot q^2_{min})) \cdot \rho t, \quad (2)$$

where $q^2_{min} = (p\theta_{min})^2$, p is a proton momentum (GeV/c), θ is a scattering angle (radian), ρ and t are a density (g/cm^3) and thickness (cm) of a nitrogen target. Formula (1) was implemented into the STRUCT code for studies of beam-nitrogen elastic scattering described in the rest of this paper with gas pressure given in a nitrogen equivalent.

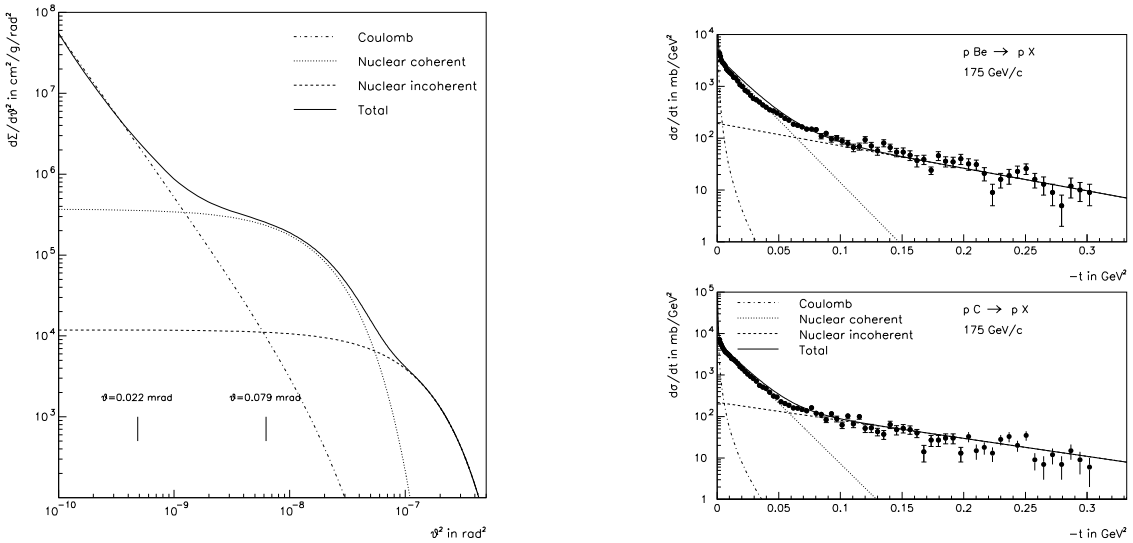

Figure 7: Components of the proton-nitrogen elastic differential cross section at 1 TeV (left) and comparison to experimental data [15] at 175 GeV/c (right).

6 Pressure Bump

A poor vacuum in a short warm region of a superconducting accelerator can considerably increase the average vacuum in the machine, lead to a high beam-gas interaction rate in such a region and, consequently, to an increased beam loss rate on limiting apertures. As took place at the beginning of the Tevatron Run II, a 2-m long region with a pressure of 3×10^{-6} torr gave rise by 10^{-9} torr to the average pressure in the ring. The effect of such a "pressure bump" on beam loss and detector backgrounds depends on its location in the ring. A rare process of a large-angle nuclear elastic beam-gas scattering can increase the proton (antiproton) betatron amplitude to a value which exceeds the Tevatron aperture. A proton (antiproton) scattered to an angle ≥ 0.079 mrad would be lost in the IP region during the first turn, if the β-function β_1 at the location of the "bump" is of the order of 100 m (see Table 2). The angle is larger for smaller β_1 (see also Fig. 7 (right)).

Table 2: Probability (2) for the angles required for protons to be lost at the Tevatron main collimators and low-β region for scattering at a 2-m long region with a pressure of 3×10^{-6} torr.

pA elastic scattering			Beam loss			
β_1	θ_{min}	Probability	Location	$R_{aperture}$	β_2	Loss rate
m	mrad	10^{-12}		mm	m	10^6 s^{-1}
100	0.022	5.79	Collimators	2	80	2.7
35	0.038	5.45	Collimators	2	80	2.5
100	0.079	4.08	Low-β quads and separators	25	1000	1.9
35	0.130	2.28	Low-β quads and separators	25	1000	1.0

The beam loss distributions calculated for such a 2-m long "pressure bump" in the F11 region with a pressure of 3×10^{-6} torr are presented in Fig. 8. Here DØRoman Pots are at 8σ and BØRoman Pots are at 10σ. The total loss rate from this process is as high as 1.6×10^{6} s^{-1}. The corresponding beam loss in the BØregion upstream of the detector is 4.4×10^{5} s^{-1} that is more than an order of magnitude higher compared to the loss rate 3.5×10^{4} s^{-1} originated by the tails from the main collimators. For the DØregion, the "pressure bump" gives 4.8×10^{4} s^{-1} to be compared to 2.4×10^{4} s^{-1} from the collimators.

Beam loss at BØand DØas a function of a "pressure bump" location in the ring, and in the region between AØand BØare shown in Fig. 9. A "bump" immediately downstream of the collider detectors produces losses which are three orders of magnitude lower compared to the maximum rate from the "bump" at about 1000 m upstream. The collimation system with its small aperture of 5-6 $\sigma_{x,y}$ protects well from the beam-gas induced losses upstream of it.

Beam loss rate in BØas a function of a "pressure bump" location in the region between AØand BØis shown in Fig. 10 along with a function of $\| \beta_1^{1/2} \cdot sin\varphi \|$ at the location of the bump. The value $\| x' \cdot \beta_1^{1/2} \beta_{separator}^{1/2} \cdot sin\varphi \|$ is a particle displacement in the $p\overline{p}$ orbit separators upstream of the IP for a particle scattered to the angle of x' at the "pressure bump". The peaks of a horizontal function $\| \beta_x^{1/2} \cdot sin\varphi_x \|$ coincide with the peaks of beam loss in BØbecause of an additional displacement of the particles in the separators in the horizontal plane due to a nonzero dispersion.

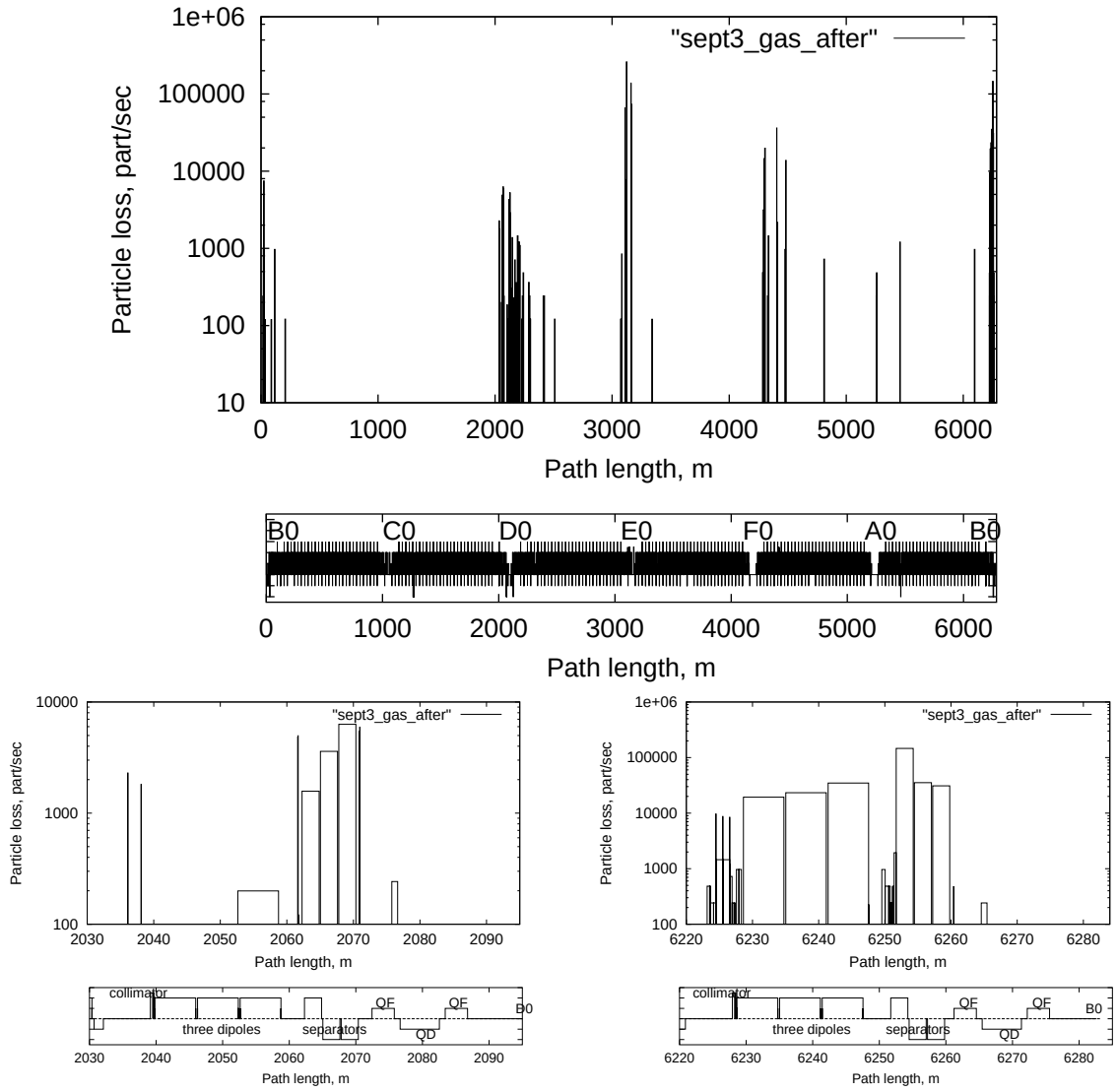

Figure 8: The “pressure bump” induced beam loss distributions in the entire ring (top) and in the DØand BØregions (bottom).

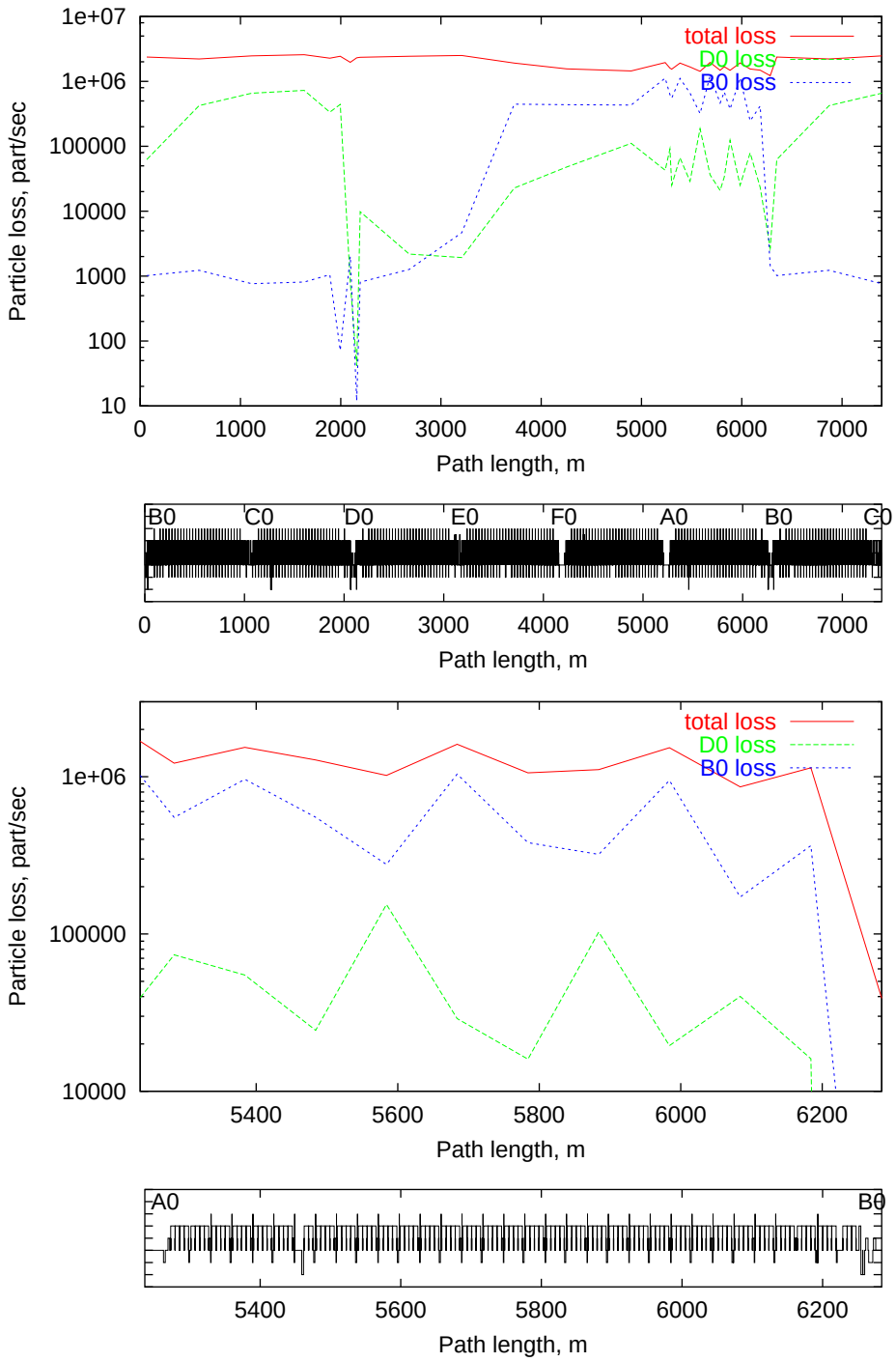

Figure 9: Beam loss at BØand DØas a function of a “pressure bump” location for the entire ring (top) and AØ-BØregion (bottom). Solid (red) line is total loss, dashed (green) is DØloss, and dashed (blue) is BØloss.

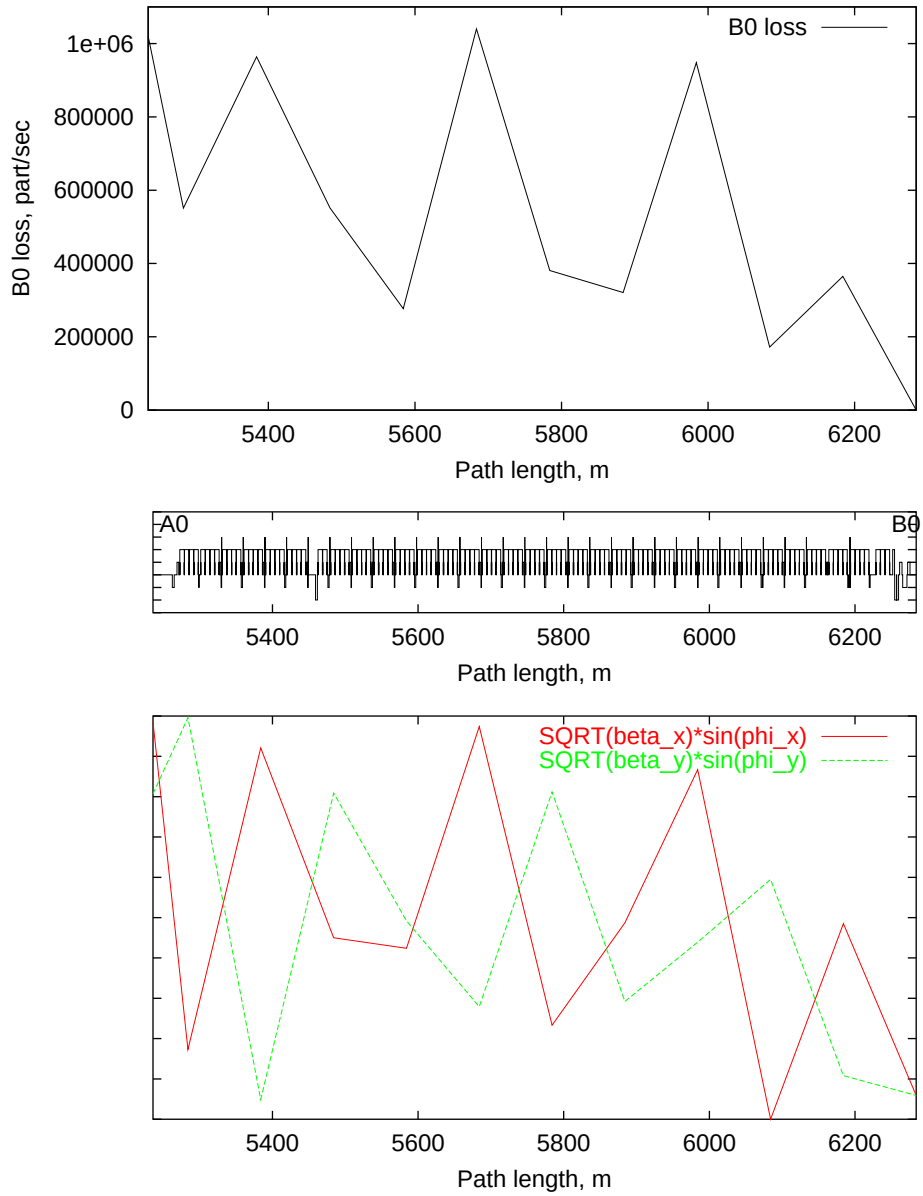

Figure 10: Beam loss at BØas a function of a “pressure bump” location in the AØBØregion (top) and $\| \beta^{1/2} \cdot sin\varphi \|$ at the locations of a “pressure bump” (bottom, with solid (red) line for horizontal and dashed (green) for vertical planes).

7 Uniformly Distributed Pressure

With a uniform distribution of a residual gas pressure, the locations of beam interactions with gas are randomly distributed around the accelerator circumference. The simulations show that the beam loss rate in the detector regions depends linearly on the gas pressure. Beam loss rate upstream of DØand BØ as a function of an average gas pressure is shown in Fig. 11 along with a loss rate originated by the collimation system. The later – to the first approach – is independent of a gas pressure. The reason is that in the Tevatron, the transverse emittance growths is mainly related to the intrabeam scattering with a rather modest contribution from beam-gas interactions. A nuclear elastic beam-gas scattering at a gas pressure $\geq 2\times 10^{-10}$ torr exceeds the beam loss in the IPs created by tails from the main collimators. Most of the particles are lost in the separators and in the three dipoles preceding the IPs.

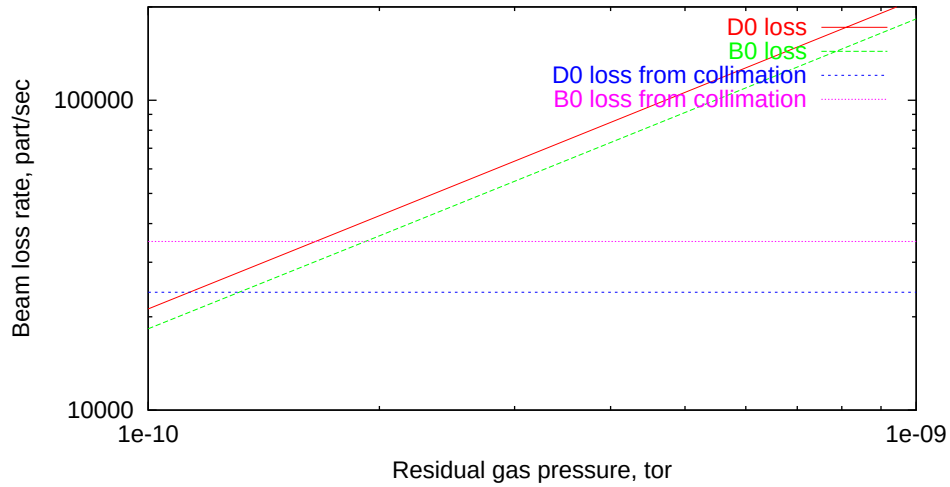

Figure 11: Beam loss rate upstream of DØ(solid (red)) and BØ(dashed (green)) as a function of an average gas pressure. Also shown are beam losses upstream of DØ(dotted (blue)) and BØ(solid (magenta)) originated by the collimation system.

8 Shadow Collimators

We found that a system of shadow collimators (masks) placed at a π phase advance upstream of the separators and immediately upstream of the last three dipoles would allow to suppress the beam-gas induced beam loss in the IPs by an order of magnitude. The best protection is provided by a system of three masks for each of the IPs as shown in Fig. 12 for BØ. First two collimators are placed at a π phase advance in horizontal and vertical planes, and a third one is in a few degrees with respect to the separators. A significant protection of the IPs can be achieved with a reduced system of two or even one masks. Beam loss distributions in the DØand BØregions without shadow collimators and with different combinations of such masks are shown in Fig. 13 for the average residual gas pressure in the ring of 10^{-9} torr. A combination of all six collimators (three for each of the IP) positioned at $13\sigma_{x,y}$ gives the maximum suppression of beam loss in the IPs. It turns out that a combined *xy*-collimator (in each IP) positioned at $13\sigma_x$ ($\pm$11 mm) and $20\sigma_y$ ($\pm$6.3 mm) and located upstream of the last three dipoles gives almost the same result.

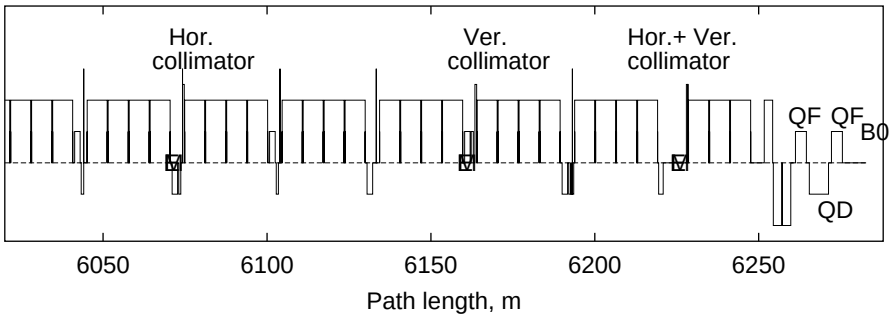

Figure 12: Location of shadow collimators upstream of BØ

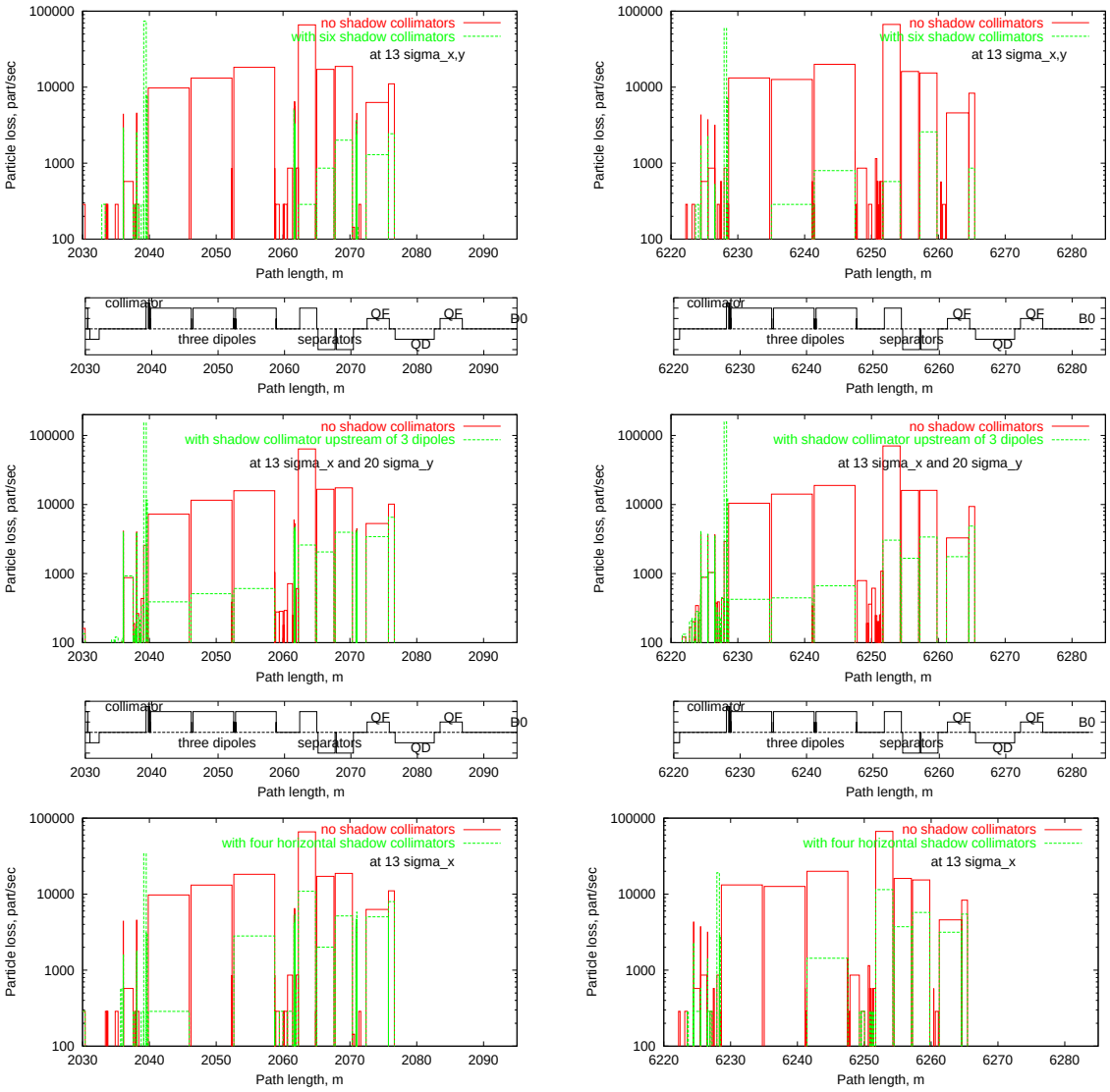

Figure 13: Beam loss distributions in the DØand BØregions without shadow collimators and with three masks (top), one combined *xy*-mask (middle) and two masks (bottom) (all for each IP). Solid (red) histograms are without masks, dashed (green) histograms are with masks.

A BØshadow collimator installed at $13\sigma_x$ and $20\sigma_y$ at A48 upstream of the last three dipoles would reduce the beam-gas induced backgrounds in the CDF and DØmain detectors and – as shown in Ref. [16] – protect the CDF silicon detectors in an accidental event of an abort kicker prefire (AKP). The optimal positions of such a collimator for a proton beam are x = 9.2 mm and y = 4.4 mm at the non-IP side of the Roman Pots station (upstream RP) or x = 11.1 mm and y = 6.3 mm at the IP side of the RP station (downstream RP). In the last case, the RPs do not suffer from the background generated in the mask by beam halo [17], but unfortunately, such a mask would decrease the RP horizontal acceptance. Additional concern is the background at RP from secondaries originated in the mask by the antiproton beam halo and antiprotons scattered in the IP to a large angle. This background can not be removed from the statistics as it has the same time as the registered particles. Therefore, the mask in this case can have only three jaws (Fig. 14) or it should go to the non-IP side of the RP station with the extra background removed from statistic by timing (different time for proton halo and antiprotons scattered in the IP). The protection efficiency of the mask at the IP end of the RP station is several times lower because of its larger aperture. The results of calculations presented below are related to the collimator placed at the non-IP end of the CDF and DØRoman Pots, i.e., upstream of the RPs for the proton beam.

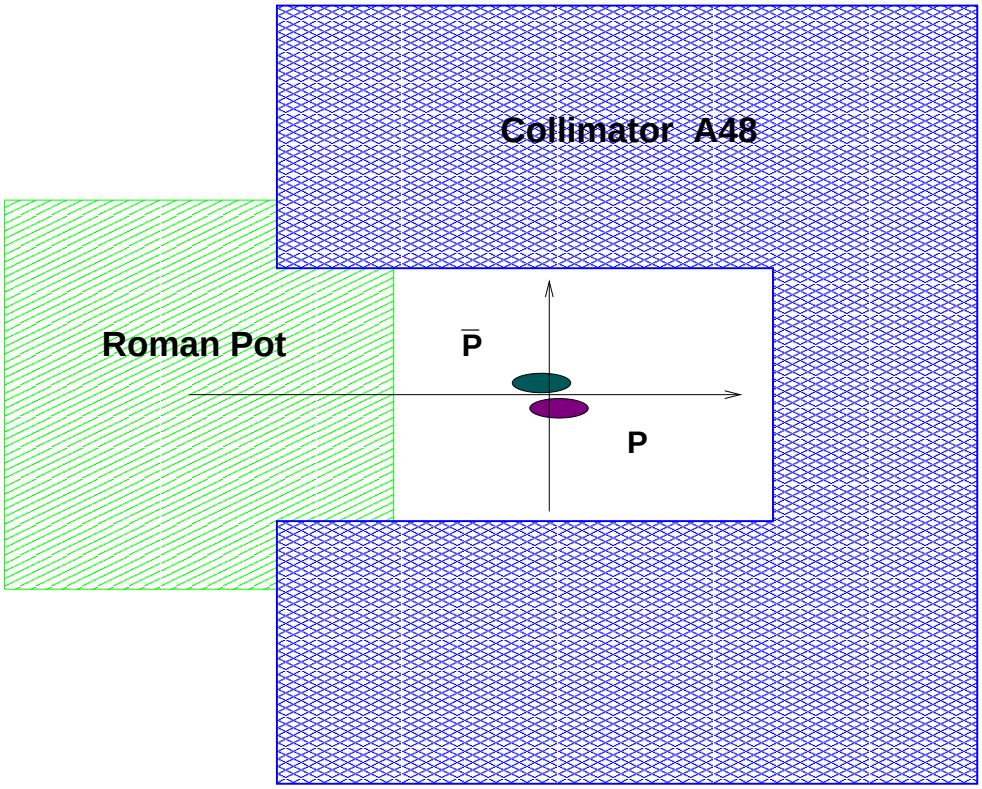

Figure 14: Shadow collimator at the IP end of the Roman Pots station.

9 Realistic Pressure Distribution

Residual gas pressure distribution in the Tevatron Run II has been measured by Bruce Hanna [18]. Fig. 15 shows these results along with a calculated rate of proton interactions with gas and corresponding beam loss distribution in the ring. The distributions exhibit the same behavior.

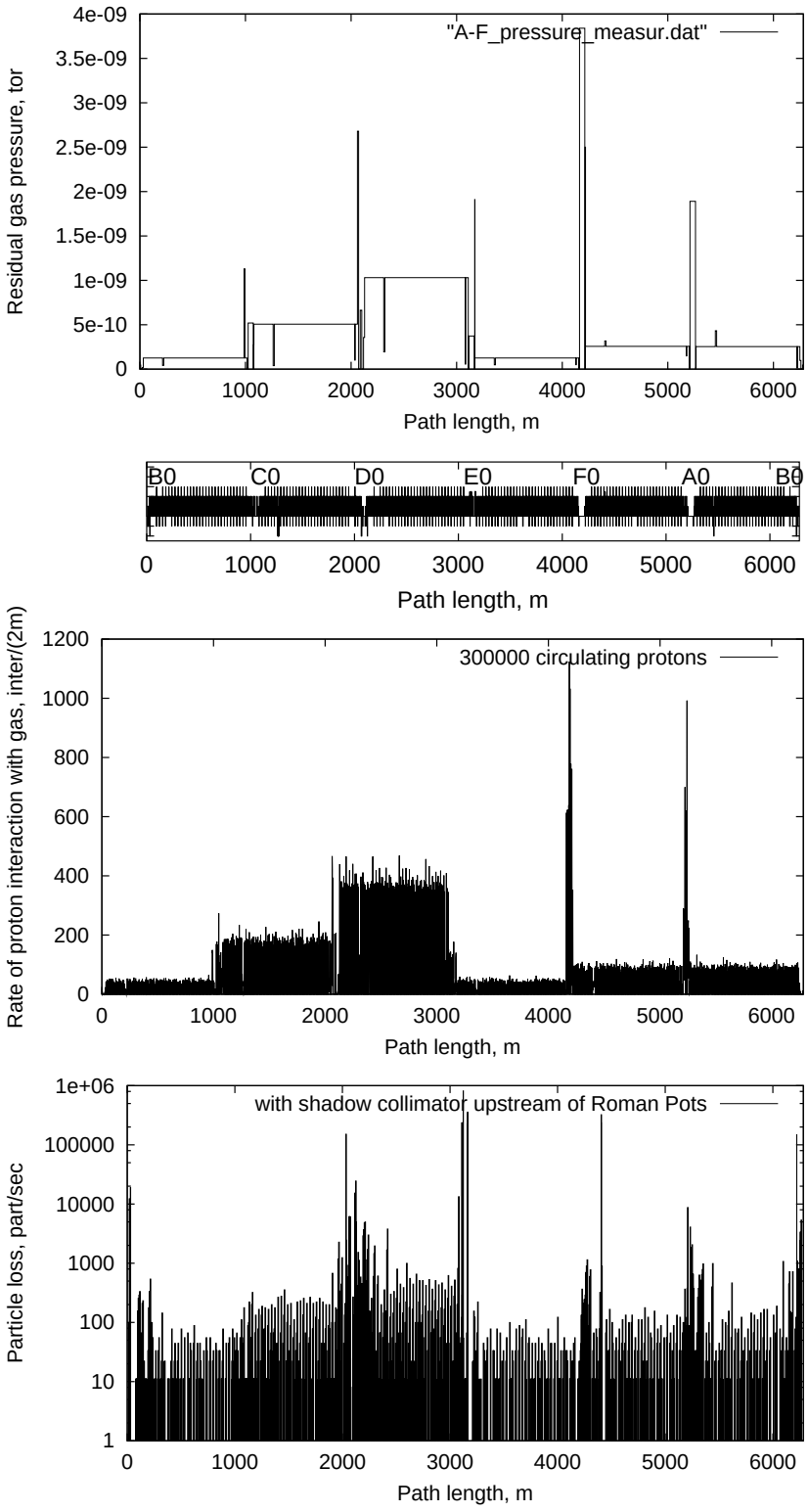

Figure 15: Measured [18] residual gas pressure (top), rate of proton interactions with gas (middle) and beam loss distribution in the Tevatron ring from nuclear elastic beam-gas scattering (bottom).

Details of beam loss distribution in the DØand BØregions are shown in Fig. 16 with and without the $13\sigma_x$ - $20\sigma_y$ shadow collimators at the non-IP ends of the RP stations. The loss rates from the warm regions are 3 to 7 times less compared to the rates from the cold regions. The C-arc cold region with an average pressure of 5×10^{-10} torr and the C49 warm region with a pressure of 2.7×10^{-9} torr are responsible for the beam loss in the DØregion. The loss rate upstream of DØis equal to 1.75×10^{5} s^{-1}. The D-arc cold region with an average pressure of 10^{-9} torr and the warm regions FØand AØwith average pressures of 3.8×10^{-9} torr and 1.8×10^{-9} torr, respectively, are responsible for the beam loss in the BØregion. The loss rate upstream of BØis equal to 1.30×10^{5} s^{-1}. The total calculated beam loss rate in the ring from the nuclear elastic beam-gas scattering is 2.87×10^{6} s^{-1}, that is about 10% of that intercepted by the collimation system from all other sources.

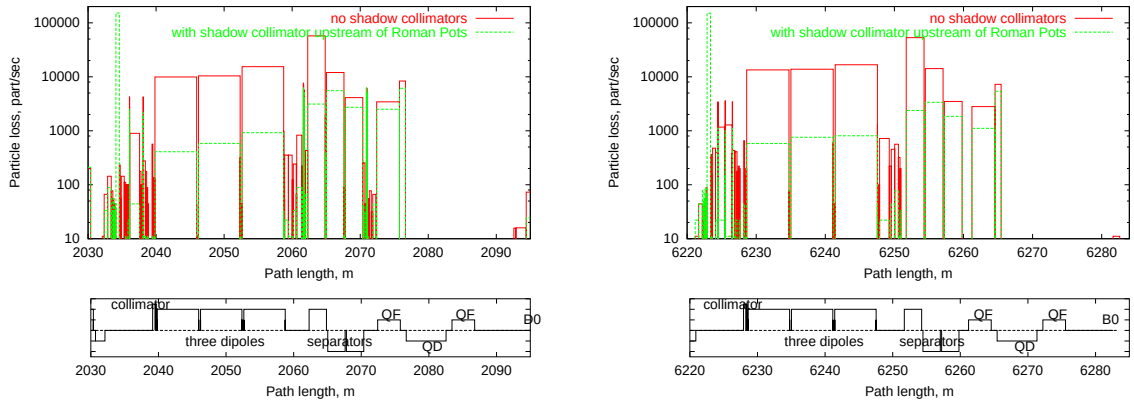

Figure 16: Beam-gas induced loss distributions in the DØand BØregions without (solid (red)) and with (dashed (green)) a shadow collimator at $13\sigma_x$ and $20\sigma_y$ at the non-IP ends of the RP stations at the measured residual gas pressure [18].

10 Beam Loss Partition

Beam loss distributions in the DØand BØregions due to nuclear elastic beam-gas scattering and large angle Coulomb scattering – both at the average gas pressure in the ring of 10^{-9} torr – are presented in Fig. 17 and Table 3 in comparison with those due to elastic $p\overline{p}$ interactions at the two IPs. As shown in Fig. 7 (left), at angles responsible for beam loss in the interaction regions ($\theta \geq 0.079$ mrad), the Coulomb scattering cross section is more than an order of magnitude smaller than the nuclear elastic cross sections. As a result, a direct contribution of the beam-gas Coulomb scattering to the beam loss in DØand BØis negligible with the nuclear coherent scattering being a driver (with a contribution from nuclear incoherent scattering). Upstream of the both collider detectors, the beam loss rates originated directly from the beam-gas Coulomb scattering and elastic $p\overline{p}$ interactions are two orders of magnitude less compared to the coherent and incoherent beam-gas nuclear scattering.

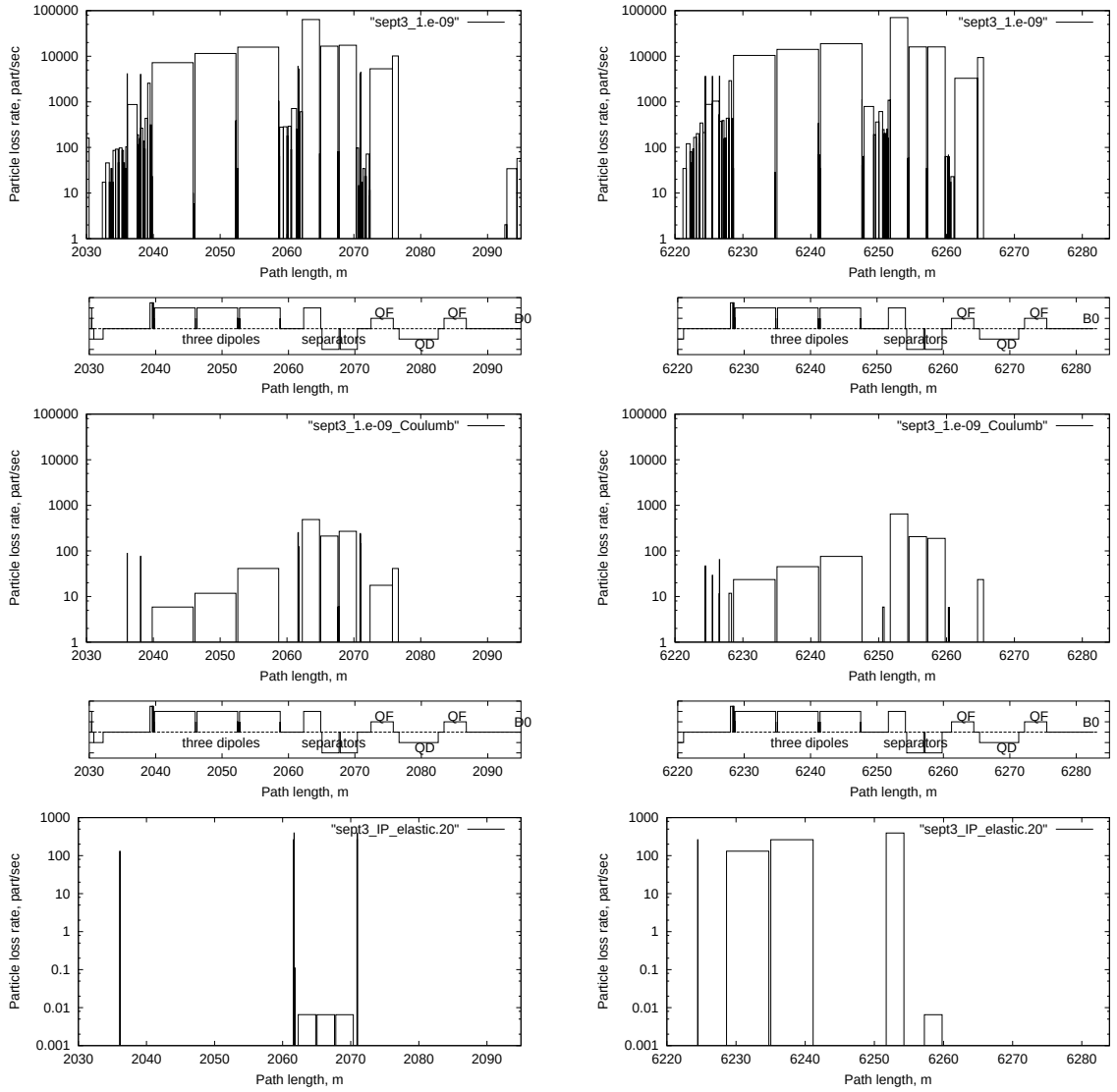

Figure 17: Beam loss distributions upstream of DØand BØfor nuclear elastic beam-gas scattering at uniform gas pressure distribution 10^{-9} torr (top), large angle Coulomb scattering (middle), elastic $p\overline{p}$ interactions at two IPs (bottom).

Table 3: Beam loss rates upstream of DØand BØfor three sources of particle scattering.

Source	Beam loss rate, s^{-1}	
	upstream of DØ	upstream of BØ
Nuclear elastic beam-gas	2.04×10^{5}	1.87×10^{5}
Large angle Coulomb beam-gas	2.72×10^{3}	1.40×10^{3}
Elastic $p\overline{p}$ at two IPs	1.44×10^{3}	1.05×10^{3}

Fig. 18 from Ref. [17] shows contributions of the three components – tails from collimators, beam-gas inelastic interactions at 7×10^{-9} torr in the vicinity of CDF and beam-gas elastic scattering – to the background rates in the CDF West beam halo monitors (BHM) for two values of the average gas pressure for elastic scattering for incoming protons. The BHM are about 60 cm around the beam pipe, at 18 m from the IP. Of course, partial accelerator-related background rates are different for different CDF and DØsubdetectors. Fig. 19 shows a distribution of protons hitting the shadow collimator (mask) for elastic beam-gas scattering and tails from the main collimators. One sees how nicely the mask intercepts the elastically scattered protons dominating in this case over those outscattered from the secondary collimators.

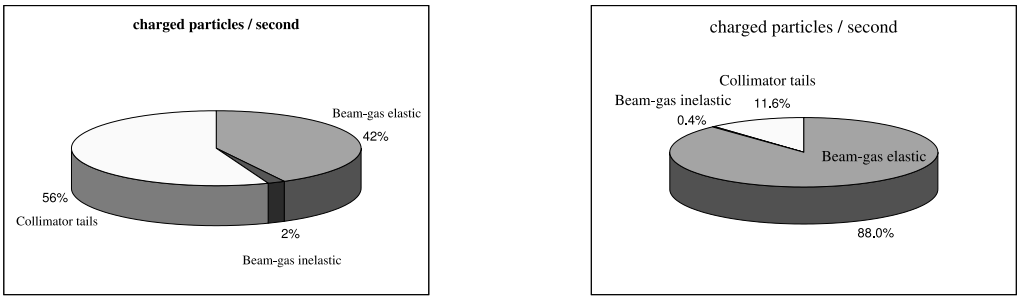

Figure 18: Contribution to BHM backgrounds at average pressure in Tevatron of 10^{-10} (left) and 10^{-9} (right) torr.

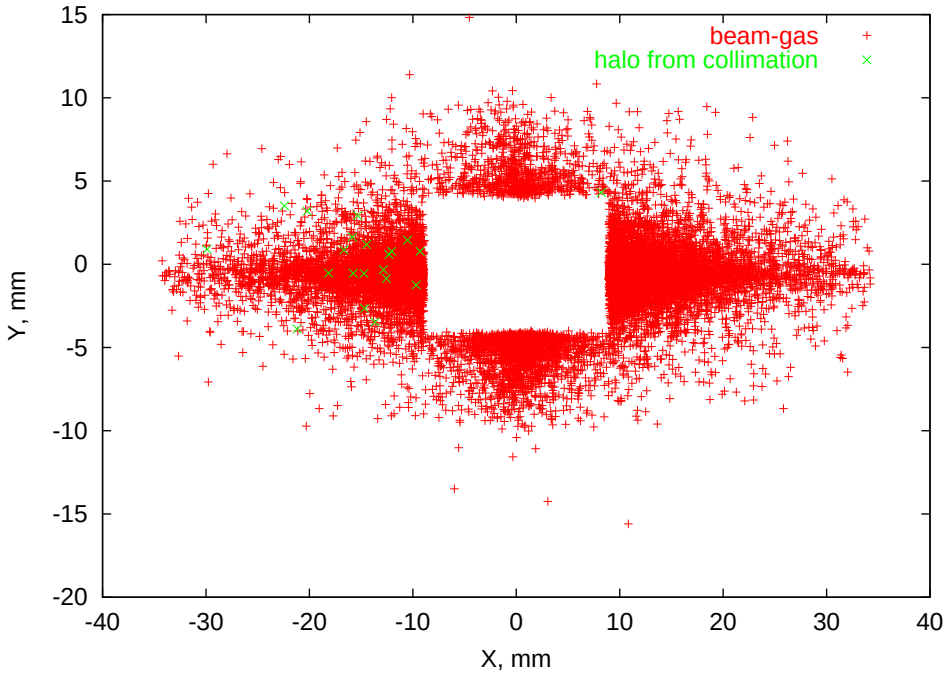

Figure 19: Proton hits at the “double L-shape” A48 collimator from elastic beam-gas interactions in the ring (red pluses) and tails from the main collimators (green crosses).

11 Backgrounds in CDF and DØ

Substantial efforts have been put to build a detailed MARS14 [6] calculational model in the BØand DØregions. It includes [17] the CDF detector with its experimental hall (Fig. 20), a simplified DØregion and $\pm$150 m of the Tevatron structures around BØand DØwith quadrupoles, dipoles, separators, Roman Pots, tunnel and surrounding dirt. It is used for realistic simulations to investigate short- and long-range effects of beam loss on backgrounds and radiation levels in the CDF and DØsubdetectors. The CDF dipole Roman pots (RP) set is composed of three detectors one meter apart from each other and starts with RP3 located at 58.6 m from the IP, for an incoming proton. The RP horizontal edge is at 12 mm from the beam pipe axis. The scintillator part of the RP facing the beam is 2×2 cm^2. The DØRoman Pots have the same sensitive area 2×2 cm ^{2} but are based on the optical fiber technology.

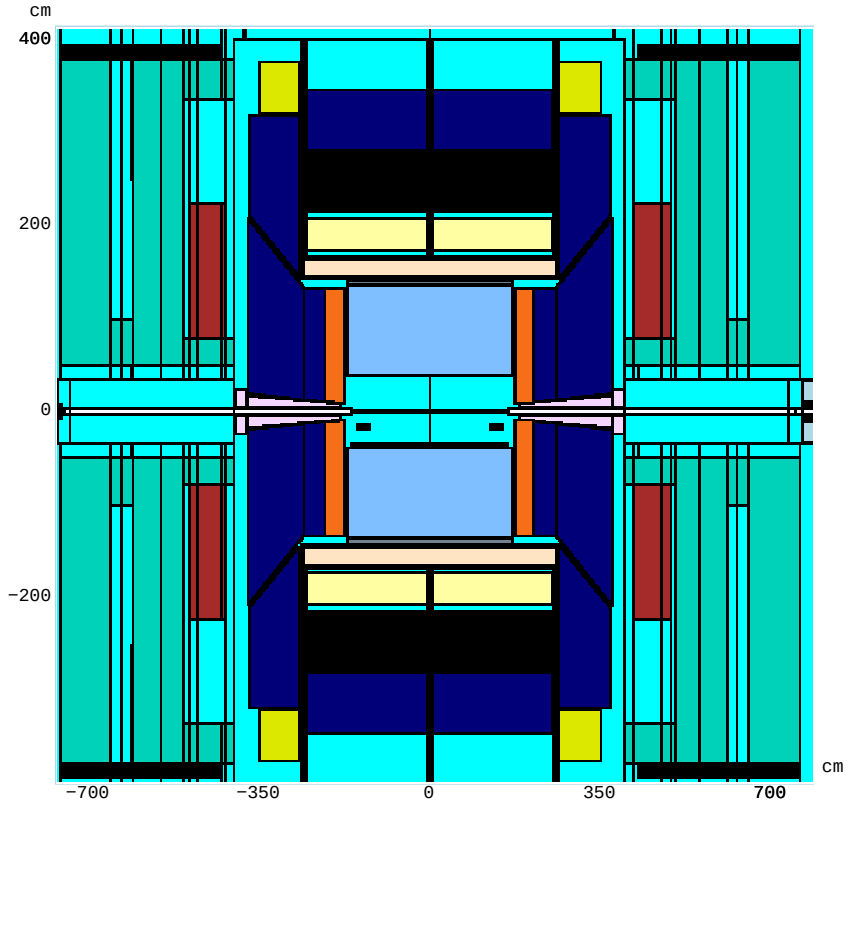

Figure 20: The CDF MARS model.

Several shapes and lengths were investigated for optimization of the BØand DØshadow collimator such as an aperture of 18.3 mm$\times$8.7 mm for “double L-shape”, “single L-shape” and “mini-bar” A48 collimators. For the “single L-shape” version, the bottom part of the “double L-shape” version remains as well as the vertical right part. The aim is the most effective protection of CDF in the event of an AKP with simultaneous minimization of halo generated backgrounds in the RP. Energy cut-offs in the MARS runs were 200 keV for all particles except neutrons with a threshold of

100 keV.

Fig. 21 (left) shows MARS-calculated charged particle flux in the CDF BHM with and without the "double L-shape" A48 collimator. The calculations were done with all the components of the beam loss source term, with an average pressure for elastic scattering of 10^{-10} torr. One sees that the collimator reduces the rates up to one order of magnitude. The results without collimator are used to compare with recent measurements by Rick Tesarek [19]. Fig. 21 (right) compares his data with corresponding MARS results. A reasonable agreement is found. A small offset on the counter axis between measurements and simulation is to distinguish the points.

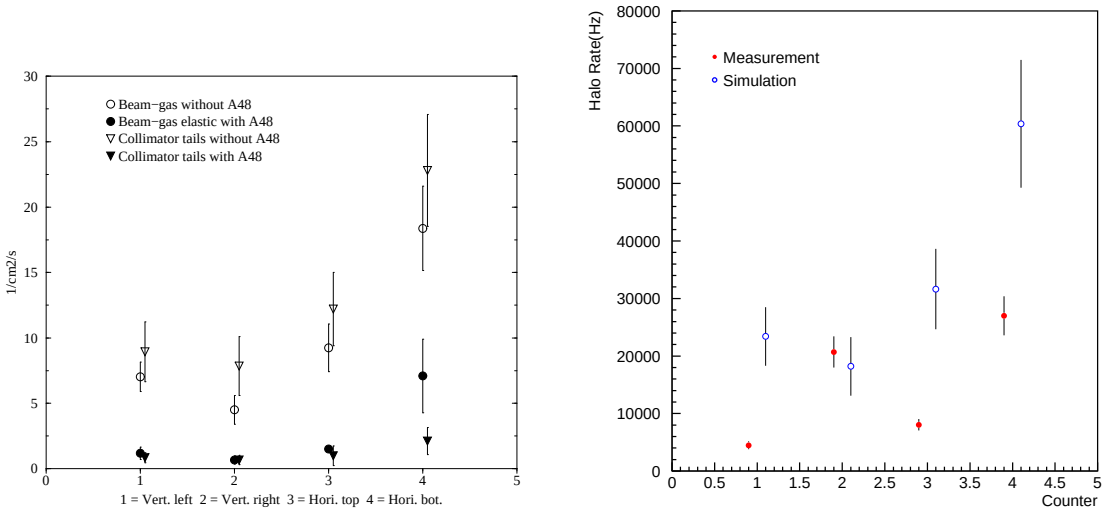

Figure 21: CDF BHM hit rate with and without A48 collimator (left) and corresponding comparison of MARS calculations with data [19] without the collimator (right).

12 Roman Pots

Shadow collimators (masks) implemented in the vicinity of the CDF and DØRoman Pots would certainly affect their performance [17]. First question is the dose that the RP would receive due to low-energy particles generated in the collimator and if this would cause a premature degradation and affect the lifetime of the scintillator (silicon). Fig. 22 shows the rates in the RP with a "double L-shape" A48 collimator of different lengths due to beam halo interactions (left) and a single event of a kicker prefire AKP with a bunch of 2.78×10^{11} protons on A48 (right). The beam-gas elastic contribution is calculated for 10^{-9} torr on average. With a 0.5-m steel collimator (3 interaction lengths), 0.01 rad/s is an upper limit for the absorbed dose rate in the scintillator. With a 10^7 second physics year, it corresponds to 100 krad/yr. This is to be compared to 20 krad per a single AKP. Note, that good scintillators can withstand about 1 Mrad.

Another issue is the background that would disturb or deteriorate the diffractive physics studied with the RP. Fig. 23 shows spatial distributions of the primary hits on the CDF RPs without a shadow collimator A48. Only charged particle flux in the RP sensitive volume is of interest here. The total primary hit rate is 1.94×10^5 s^{-1} through a 4 cm^2 area. The peak primary proton flux is about 5×10^5 cm^{-2} s^{-1}. One of the concerns is the number of antiprotons coming from the IP and passing through the RP that would hit the collimator and then be backscattered towards the pots again.

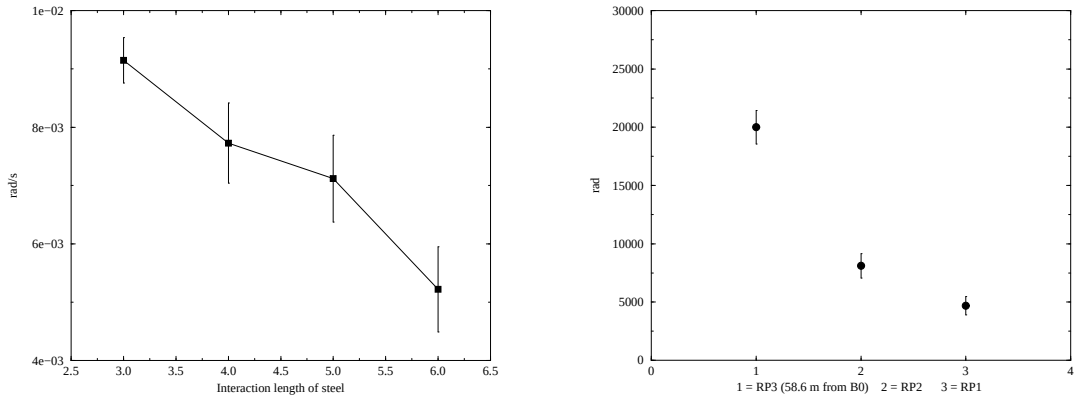

Figure 22: Absorbed dose in RP3 due to beam halo (left) and dose in RP1-RP3 due to AKP (right).

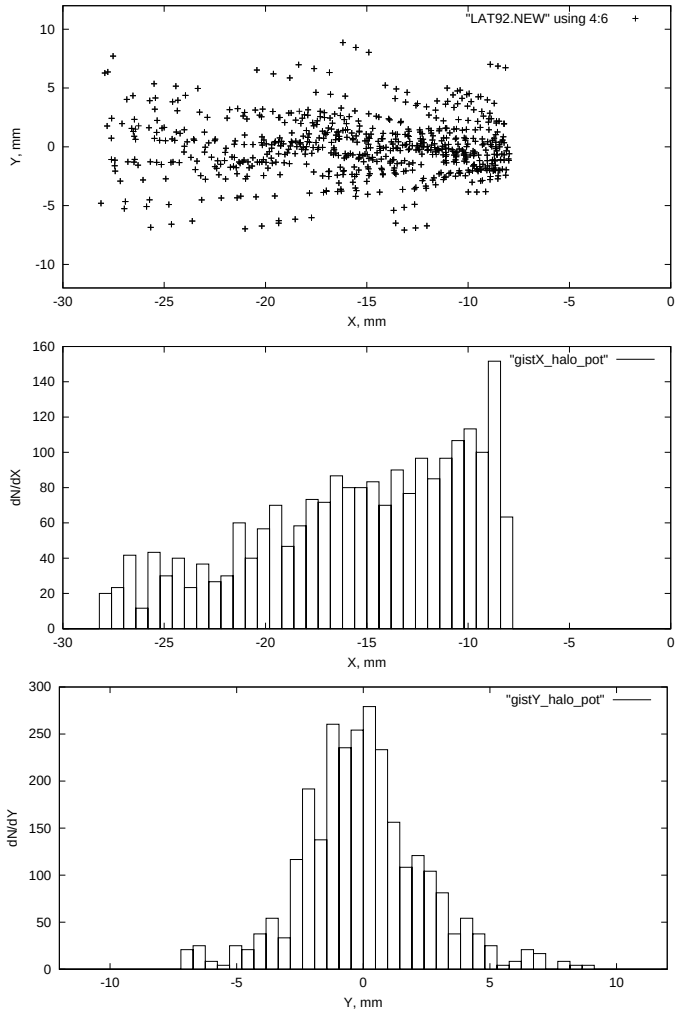

Figure 23: Halo hit distributions in the CDF Roman Pots without shadow collimators.

A simple MARS14 simulation has been performed with a 1-TeV beam on a 0.5-m long steel mask. Two detectors were modeled, first 1 m upstream of the mask, second 1 m downstream. The charged particle flux normalized to 1 proton is shown on Fig. 24 and include primaries and secondaries. The radius in the abscissa represents the distance with respect to the initial beam axis. It appears that counts in the RP due to albedo would represent a tiny fraction of the background. At a 2.5 cm radius from the initial proton beam, for the worst case, the ratio albedo/forward is roughly 0.001.

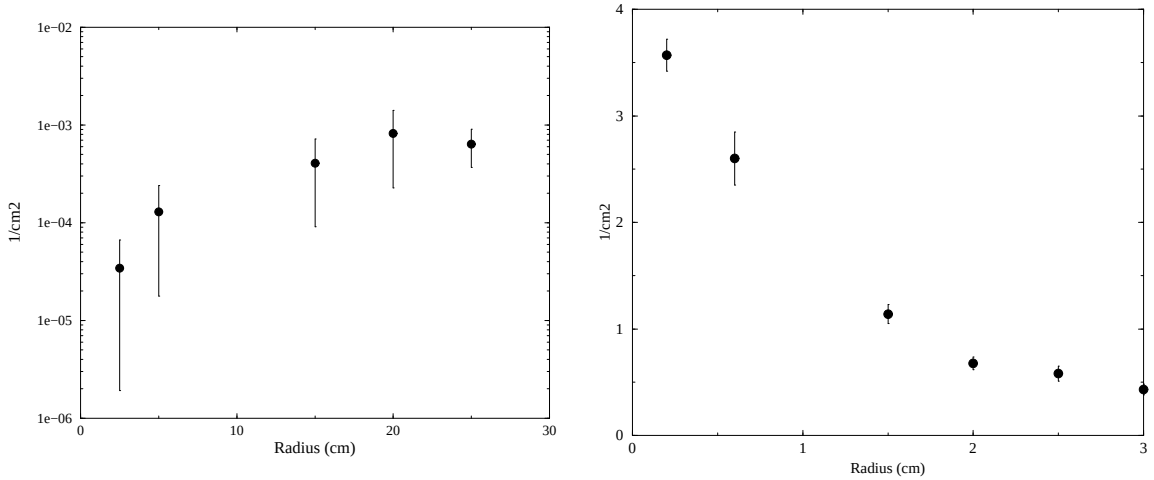

Figure 24: Charged particle albedo (left) and forward (right) flux in RP with a 0.5-m long steel rod.

Table 4: Primary proton hit rates (in 10^5 s^{-1}) in the CDF A48 mask and Roman Pot RP3 due to tails from the main collimators and nuclear elastic beam-gas scattering for two distances of the CDF RPs from the beam, 10 and 15σ_x.

	Without A48 and C48 masks		With A48 and C48 masks		With A48 mask only
	10σ	15σ	10σ	15σ	15σ
Tails					
A48	-	-	0.335		0.330
RP3	0.358	0.196	0.087	0.010	0.014
Beam-gas					
A48	-	-	1.620		1.636
RP3	0.870	0.395	0.282	0.014	0.014

Results on halo induced hit rates in the CDF and DØRoman Pots are presented in Tables 4 and 5 for both sources – tails from the main collimators and beam-gas elastic scattering at the average gas pressure of 10^{-9} torr – with and without shadow collimators (masks). The secondary collimators of the main collimation system are at $6\sigma_{x,y}$, DØRPs are at $8\sigma_{x,y}$ and $10\sigma_{x,y}$ (ROMAD1,3), and CDF RPs are at $15\sigma_{x,y}$.

Simulations have been done to compare the charged particle flux reaching RP3 with the different shapes described earlier. The stainless steel collimator length was varied from 0.5 to 1 m, or 3 to 6 nuclear inelastic interaction lengths. This would leave at least 0.5 m of space between the end of A48 and RP3. Fig. 25 (left) shows the effect of the length and shape of the mask on the rate of charged particles in the RP3 calculated at 10^{-9} torr average pressure for beam-gas elastic scattering.

Table 5: Primary proton hit rates (in 10^5 s^{-1}) in the CDF and DØRoman Pots due to tails from the main collimators and nuclear elastic beam-gas scattering.

	Tails		Beam-gas	
	Without mask	With mask	Without mask	With mask
ROMAD1	0.306	0.237	1.322	1.278
ROMAD3	0.332	0.267	1.321	1.284
ROMA1Su	1.240	1.216	2.385	2.548
ROMA1Sd	1.715	1.732	1.988	1.941
ROMA2Su	0.0	0.001	1.421	1.413
ROMA2Sd	0.001	0.004	1.625	1.616
ROMA1Qu	1.195	1.150	1.833	1.754
ROMA1Qd	1.637	1.661	1.581	1.545
ROMA2Qu	0.0	0.001	1.209	1.198
ROMA2Qd	0.0	0.001	1.492	1.494
ROMP1Qu	1.467	1.466	1.279	1.252
ROMP1Qd	0.788	0.746	1.425	1.358
ROMP2Qu	0.013	0.010	1.610	1.595
ROMP2Qd	0.002	0.001	1.299	1.298
ROMP1Su	1.263	1.272	1.229	1.196
ROMP1Sd	1.236	1.165	1.552	1.487
ROMP2Su	0.021	0.011	1.472	1.449
ROMP2Sd	0.001	0.002	1.158	1.150
CDFPOT3	0.196	0.014	0.395	0.014
CDFPOT2	0.196	0.014	0.395	0.014
CDFPOT1	0.196	0.014	0.395	0.014

Both secondary and primary particles contribute to the hit rate here. Results for "single L-shape" and "minibar" shapes are not discernible. One could thus keep the option of a "single L-shaped" collimator. The amplification factor due to the implementation of a "single L-shape" mask of six interaction lengths of steel reaches 4.5 compared to the rates without the collimator. For a 0.5-m long "double L-shape" collimator, this difference becomes an order of magnitude (Fig. 25 (right)).

The effect of the C48 mask on the DØRoman Pots is analyzed in Ref. [17]. The loss rates upstream of DØand CDF are similar, 2.04×10^{5} p/s and 1.87×10^{5} p/s, respectively. A simple scaling allows one to obtain a prediction in the DØcase (Fig. 26 (left)). Here direct halo hits are not included and a contribution from secondaries only is shown. Direct hits are much more important for the DØRP (see Table 5), because they are closer to the beam than the CDF RP. The multiplication of secondaries due to a collimator would, however, have the same behavior and be independent of the direct hits. The shielding efficiency of a shadow collimator for representative CDF (and DØ) subdetectors is shown in Fig. 26 as a function of a distance from the IP for elastic beam-gas scattering as a source. One sees that such a mask reduces the backgrounds in the main detector by a factor of 4.5 to 25, at least for the elastic beam-gas component. This later was computed for CDF but is perfectly applied to DØ The Beam Shower Counters (BSC) are about few centimeters to the beam pipe, whereas BHM is at 0.6 m and PLUG at 1 m from the beam axis.

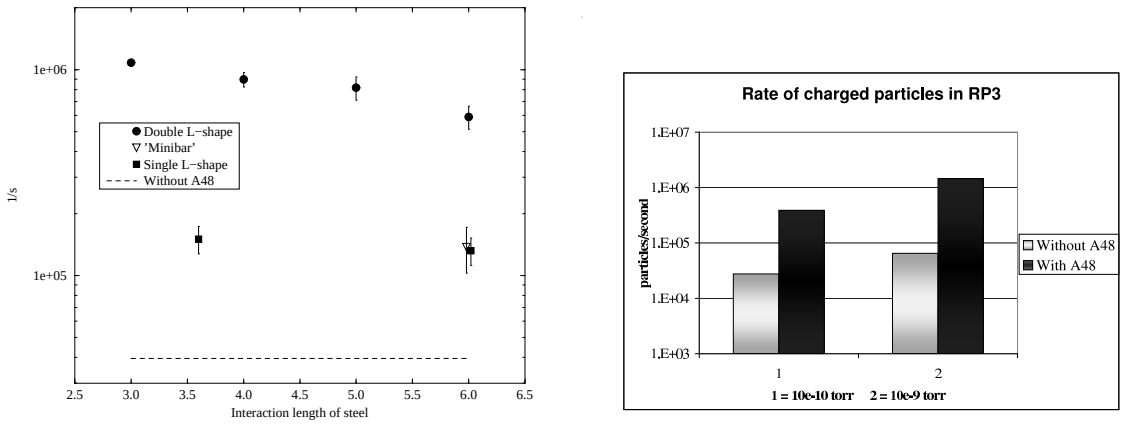

Figure 25: Rates of charged particles at RP3 as a function of the mask length for three shapes at the 10^{-9} torr average pressure (left) and their sensitivity to the gas pressure (right). The dashed line corresponds to a case without the mask.

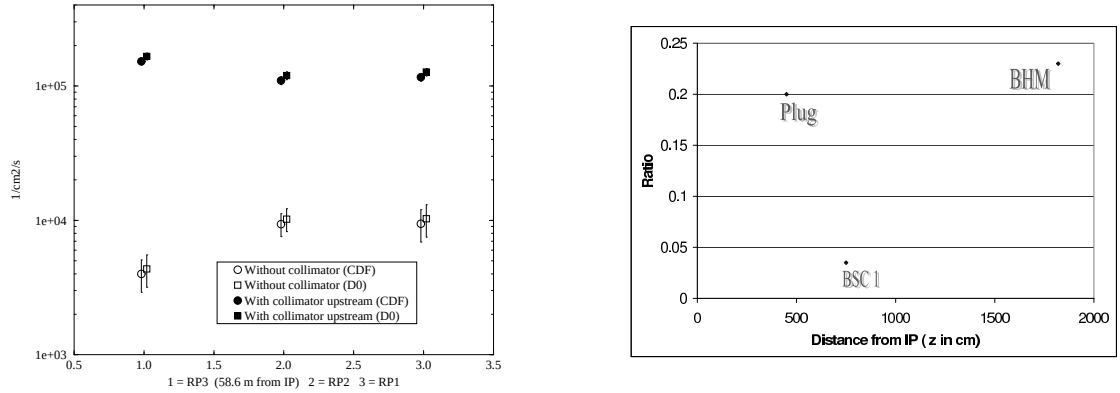

Figure 26: Charged particle flux at the DØRoman Pots (left) and the main detector absorbed dose ratio with/without "double L-shaped" collimator for the elastic contribution as a function of a distance from the IP (right).

13 Conclusions

A nuclear elastic beam-gas scattering in the Tevatron generates beam loss in the interaction regions not intercepted by the main collimation system designed for cleaning of slow growing beam halo (resonances, beam-gas multiple Coulomb scattering, RF noise, magnetic fields instabilities and other processes). This beam loss – and additional background in the DØand CDF detectors – is proportional to the pressure and length of warm regions in the accelerator, and depends on the location of these regions with respect to the IPs. With a 2-m long "pressure bump" of 3×10^{-6} torr, these backgrounds can exceed by an order of magnitude those due to tails from the main collimation system. They are comparable at an average gas pressure in the machine of about 2×10^{-10} torr. A proposed system of shadow collimators placed in a phase advance of π upstream of the separators would protect the CDF detector against AKP accidents and suppress the beam loss in the IPs caused by beam-gas interactions by an order of magnitude. Corresponding backgrounds in the main DØand CDF detectors are also reduced ten times. One still needs to find a way to suppress the extra background in the Roman Pots generated in the shadow collimators.

14 Acknowledgments

We are thankful to M. Albrow, A. Brandt, B. Hanna, R. Moore, R. Tesarek and I. Tropin for useful discussions.

References

[1] M.A. Maslov, N.V. Mokhov, I.A. Yazynin, "The SSC Beam Scraper System", SSCL-484 (1991).

[2] A.I. Drozhdin, N.V. Mokhov, R. Soundranayagam, J. Tompkins, "Toward Design of the Collider Beam Collimation System", SSCL-Preprint-555 (1994).

[3] A.I. Drozhdin, N.V. Mokhov, "Detector-Accelerator Interface Studies at the Tevatron", *Proc. LAFEX Int. School on High Energy Physics, Lishep98 Diffractive Physics*, Rio de Janeiro, Brazil, February 16-20, 1998; Fermilab-Conf-98/105 (1998).

[4] M.D. Church, A.I. Drozhdin, A. Legan, N.V. Mokhov, R.E. Reilly, "Tevatron Run-II Beam Collimation System", *Proc. 1999 Particle Accelerator Conf.*, pp. 56-58, New York, March 29 - April 2, 1999; also Fermilab-Conf-99/059 (1999).

[5] I.S. Baishev, A.I. Drozhdin, N.V. Mokhov, "STRUCT Program User's Reference Manual", SSCL–MAN–0034 (1994); http://www-ap.fnal.gov/∼drozhdin/

[6] N.V. Mokhov, "The MARS Code System User's Guide", Fermilab-FN-628 (1995); N.V. Mokhov, O.E. Krivosheev, "MARS Code Status", *Proc. Monte Carlo 2000 Conf., pp. 943-948*, Lisbon, October 23-26, 2000; Fermilab-Conf-00/181 (2000); http://www-ap.fnal.gov/MARS/.

[7] N.V. Mokhov, V.I. Balbekov, "Beam and Luminosity Lifetime", in *Handbook of Accelerator Physics and Engineering, 2nd Printing*, Ed. A.W. Chao, M. Tigner, p. 218, World Scientific (2002).

[8] L. Burnod, J.B. Jeanneret, "Beam Loss and Collimation in the LHC: A Quantative Approach", CERN-SL/91-39 (1991).

[9] J.M. Butler, D.S. Denisov, H.T. Diehl, A.I. Drozhdin, N.V. Mokhov, D R. Wood, "Reduction of Tevatron and Main Ring Induced Backgrounds in the DØDetector", Fermilab-FN-629 (1995).

[10] J.A. Johnstone, Tevatron optics with magnet moves for Roman pots at CDF, FERMILAB-TM-2157, Aug 2001.

[11] P. Bagley, Beam Separation for the Tevatron Run-II. Private communication, December 1997.

[12] G. Jackson, D. Finley, R. Johnson et al., "Luminosity Lifetime in the Tevatron", Fermilab-Conf-88/80 (1988).

[13] T. Risselada, The Effect of the Betatron Tune on the Impact Parameter at LHC Primary Collimators, CERN SL/Note 92-16(AP) (1992).

[14] M. Seidel, Determination of Diffusion Rates in the Proton Beam Halo of HERA, DESY-HERA 93-04 (1993).

[15] A. Schiz et al. *Phys. Rev.*, **D21**, 3010 (1980).

[16] A.I. Drozhdin, M.D. Church, "Tevatron Abort Kicker Prefire Simulations", *to be published*.

[17] L.Y. Nicolas, N.V. Mokhov, A.I. Drozhdin, "MARS Simulation of Beam Loss and New Collimator Impact on the CDF and DØSubdetectors", DØNote-4129 (2003), CDF-Note-6407 (2003).

[18] B. Hanna, Residual Gas Pressure Measurements, August 2002.

[19] http://ncdf67.fnal.gov/∼tesarek/radiation/.